CHAPTER XXIX-2

INTERNAL STRUCTURE OF THE FEMURS AND TIBIA

Virginie VOLPATO, Arnaud MAZURIER,
Laurent PUYMERAIL & Roberto MACCHIARELLI

Abstract

The adult Neandertal partial skeleton Spy II preserves the right and left femurs (Spy 8 and 16) and the complete left tibia (Spy 9). By using advanced techniques of virtual modeling and quantitative analysis applied to their tomographic (CT) record, we characterised the endostructural shaft morphology of the three lower limb elements, assessed the degree of volumetric bilateral asymmetry of the femurs and the textural characteristics of their proximal ends, and explored the inner organisation of the tibial plateau.

The three shafts typically show thick cortical bone and reduced medullary cavity. The assessment of cortical thickness topographic variation along the femoral diaphyses and their degree of bilateral asymmetry in bone volume distribution confirm that Spy 8 and Spy 16 belong to the same individual, characterised by areas of cortical strengthening (especially medio-laterally) which basically trace the topography of major muscular insertions. The hyper-thick cortico-trabecular complex of the tibial plateau, notably at the level of the medial condyle, testifies to strenuous levels of physical activity experienced by this young adult Neandertal individual.

INTRODUCTION

External and internal diaphyseal gross morphology of the lower limb long bones reflects habitual mechanical loads related to levels and patterns of physical activity associated to subsistence strategies, as well as adaptive changes during growth in locomotion modes, and, likely, climate adaptation (e.g. Ruff *et al.*, 1993, 1994; Stock & Pfeiffer, 2001, 2004; Churchill & Schmitt, 2002; Weaver, 2003; Sládek *et al.*, 2006; Stock, 2006; Cowgill & Hager, 2007; Sparacello & Marchi, 2008). At site-specific endostructural level, as the topographic variation of the cortical bone distribution and patterning of the trabecular network tend to conform in order to face the most frequently experienced functionally-related strains, measures of thickness variation of the cortical shell and trabecular struts, of bone volume fraction, and of textural anisotropy provide direct information about the nature, direction, and magnitude of the habitual loads and, indirectly, about the dynamic relationships between the individual lifestyle and its biomechanical environment (Dalstra & Huiskes, 1995; Odgaard, 1997; Odgaard *et al.*, 1997; Pearson & Lieberman, 2004; Ruimerman *et al.*, 2005; Ruff *et al.*, 2006).

Relative to recent-extant humans, the Neandertal lower limb skeleton is strongly built and exhibits much greater diaphyseal robusticity, which is consistent with higher mechanical loads experienced throughout life in both immature and adult individuals (Lovejoy & Trinkaus, 1980; Trinkaus & Ruff, 1989a, 1989b, 1999a, 1999b; Ruff *et al.*, 1993, 1994; Churchill, 1998; Trinkaus *et al.*, 1998, 1999; Beauval *et al.*, 2005). Notably, the adult Neandertal femoral shaft, which on average shows subcircular mid-shaft contour, a variable development of a medial buttress, a variably prominent *linea aspera* but no evidence of true pilaster, thick cortical bone associated to reduced medullary cavity, and expansion of the periosteal surface, is reported to have greater resistance to medio-laterally-directed bending stresses, mainly on mid-diaphysis, in addition to a peculiar resistance to axial, antero-posterior, and torsional stresses (Trinkaus & Ruff, 1989a, 1999a; Churchill, 1998; Trinkaus

et al., 1998, 1999; Churchill & Schmitt, 2002; Weaver, 2003; Beauval *et al.*, 2005). Additionally, the comparatively less platycnemic Neandertal tibia, with its ovoid to amygdaloid midshaft cross-section extended antero-posteriorly, rounded anterior crest, little prominence of the lateral interosseous crest, and rounded posterior margin, also shows thickened cortical bone and greater strength in the medio-lateral plane (Lovejoy & Trinkaus, 1980; Trinkaus & Ruff, 1989a, 1989b, 1999b; Trinkaus *et al.*, 1998, 1999; Churchill & Schmitt, 2002).

Most of the morphological and biomechanical properties of the cortical shell of the Neandertal long bones seem to appear early during growth (Ruff *et al.*, 1994; Volpato *et al.*, 2007). Conversely, little information is currently available on the textural properties and architectural variation of the Neandertal lower limb cancellous network (for the adult hip bone, see Martinón-Torres, 2003; Macchiarelli *et al.*, 2007; Volpato, 2007).

The postcranial remains from the two adult Neandertal partial skeletons Spy I and Spy II, from the cave of Betche aux Rotches, in Belgium (Fraipont & Lohest, 1886, 1887), include two femurs (Spy 8 and 16) and a tibia (Spy 9), all currently allocated to the individual Spy II (Rougier *et al.*, 2004, this volume: chapter XIX; Shackelford, this volume: chapter XXIX-1). Previous investigation on the cross-sectional geometrics of these specimens (Trinkaus & Ruff, 1989b), which documented the influence on the thigh of more medio-laterally oriented bending stresses, has shown that their biomechanical properties fit the typical Neandertal condition. Relative to bone length, the variables describing bending and torsional strength and rigidity have values well above those of the recent human means for both femurs and tibia.

By using advanced techniques of (μ)CT-based three-dimensional (3D) virtual modeling and of 2-3D quantitative analysis of the cortical and trabecular bone (Macchiarelli *et al.*, 1999, 2001, 2007; Mazurier, 2006; Mazurier *et al.*, 2006; Volpato, 2007, 2008; Volpato *et al.*, 2008, 2011), here we characterise the endostructural shaft morphology of the three lower limb bones from Spy II, assess the degree of volumetric bilateral asymmetry of the femurs and the cancellous architecture of their proximal ends, and explore the cortico-trabecular organisation of the tibial plateau.

METHODS

Spy 8 and Spy 16 represent a right and a left femur, respectively, while Spy 9 is a left tibia. Spy 8 and Spy 9 are almost complete, the femur just lacking the superior part of the greater trochanter (Fraipont & Lohest, 1886, 1887; Trinkaus & Ruff, 1989b; Rougier *et al.*, this volume: chapter XIX; Shackelford, this volume: chapter XXIX-1). Conversely, its counterpart (Spy 16) is broken at midshaft, and preserves only the proximal portion.

The 3D virtual reconstruction and structural analysis of the three specimens are based on a tomographic (CT) record performed in 2005 by means of a Siemens Sensation 64 CT model by researchers at the Royal Belgian Institute of Natural Sciences, Brussels (Semal *et al.*, 2005). Sections from the original record were reconstructed and saved on Dicom format at a voxel size of 312.5 x 312.5 x 300 μm for Spy 8, of 281.2 x 281.2 x 100 μm for Spy 16, and of 209.0 x 209.0 x 300 μm for Spy 9. The final volumes have been elaborated by means of AMIRA v.4.0 (Mercury Computer Systems, Inc.). The specimens have been oriented following the standardised protocol suggested by Ruff (2002).

Both Spy 8 and 16 proximal ends have been investigated for the textural properties of their trabecular network (Parfitt *et al.*, 1987; Odgaard, 1997). The analysis has been performed by sampling four square-shaped regions of interest (ROI) identified along a coronal virtual section of each proximal diaphysis parallel to the neck axis and crossing the head center. The ROIs, which side length systematically corresponds to one-third of the vertical diameter of the neck, respectively sample: the arcuate bundle running along the upper neck (ROI 1); the medial (ROI 2) and the lateral (ROI 3) ends of the vertical bundle; and the mid-lateral neck area included between the arcuate and the vertical bundles (ROI 4) (for anatomical details, see Macchiarelli & Bondioli, 1994). On each independently segmented and binarised ROI (Spoor

et al., 1993), the following variables have been measured for textural characterisation according to the protocol described by Volpato and co-workers (2008): trabecular thickness (tb.th.), bone volume fraction (BV/TV), and degree of anisotropy (DA, and its associated coefficient of variation, cv).

The 3D cartographies of the cortical thickness distribution along the diaphysis (mapping) have been realised using a semi-automatic segmentation method, and the relative bone topographic variation has been rendered by means of a 10-stepped colour scale (thickness increasing from dark blue up to red). Depending on the preservation conditions of each specimen, the investigated area is approximately comprised between: the mid-portion of the lesser trochanter and the upper limit of the condyles, in Spy 8; the base of the lesser trochanter and the lowermost limit of the shaft portion suitable for such analysis, in Spy 16; and between the lower border of the tuberosity and the proximal margin of the fibular notch, in Spy 9.

With special reference to the development and application of advanced techniques of 3D rendering of bone inner structural morphology, it should be noted that the specimen Spy 8 was originally used by Zollikofer & Ponce de León (2001) as fossil test-case in their pioneer methodological work on shaft morphometric maps.

In the case of Spy 8 and Spy 9, the cortical (CV) and medullary (MV) volumes have been respectively quantified for the shaft portions comprised between 35 % and 50 % (distal volume) and 50 % to 65 % (proximal volume) of the estimated biomechanical length. In Spy 16 (left femoral shaft), the same variables have been assessed only for the proximal portion and their degree of asymmetry with respect to Spy 8 (right) has been quantified according to the formula: ([(max – min)/min] x 100) (Trinkaus *et al.*, 1994).

In Spy 9, the topographic distribution of the "cortico-trabecular complex" (CTC) immediately set below the two condyles of the tibial plateau has been assessed following the protocol described by Mazurier (2006; see also Mazurier *et al.*, 2007). Thickness variation of the CTC has been measured on virtual parasagittal cross-sections at regular intervals of 250 µm along the antero-posterior direction, perpendicularly to the external bony surface, by means of MPSAK package (National Prehistoric Museum of Rome; in Dean & Wood, 2003).

A whole of 1873 and 2137 measurements have been realised for the medial (MC) and the lateral (LC) condyle, respectively. The spatial structure and variability of the dataset have been investigated through the analysis of spatial covariance, or variograms (Gringarten & Deutsch, 2001; Gumiaux *et al.*, 2003). From the interpolated grid obtained thanks to Surfer v.8.04 package (Golden Software, Inc.), CTC variation has been rendered by means of a colour scale superposed to the virtually reconstructed upper view of the plateau.

RESULTS

Spy 8 and 16 (femurs)

Thanks to the good preservation quality of the proximal end inner structure of both femurs, the assessment of the textural properties of their cancellous network has been possible for all selected ROIs except the one sampling the arcuate bundle (ROI 1) of the right specimen, Spy 8, because of punctual mineral filling (Table 1).

Thickest trabeculae (tb.th.) and greatest bone volume fraction (BV/TV) are found in Spy 8, while the left one shows a slightly higher degree of textural anisotropy (DA and cv). With respect to the variable tb.th., a right structural dominance, which does not seem to reflect the influence of diagenetic changes, is evident. Also, an orientation angular difference of ~10° between the two femurs characterises the vertical bundle. Nonetheless, the two architectures substantially overlap.

The 3D virtual rendering of the inner structural topography (cortical bone thickness variation) of the two shafts in anterior and posterior view is shown in Figure 1; the related values of the distal and proximal cortical (dCV, pCV) and medullary (dMV, pMV) volumes are given in Table 2 (which also includes the same values pertaining to Spy 9).

		tb.th.	*BV/TV*	*DA*	*cv*
Spy 8	ROI 1	-	-	-	-
	ROI 2	816	54.85	0.208	0.293
	ROI 3	884	53.61	0.219	0.287
	ROI 4	880	68.73	0.237	0.347
Spy 16	ROI 1	844	59.43	0.205	0.221
	ROI 2	728	48.67	0.240	0.340
	ROI 3	770	54.24	0.291	0.394
	ROI 4	773	61.06	0.226	0.289

Table 1. Quantitative characterisation of the textural properties of the cancellous network measured at the proximal end of Spy 8 (right) and Spy 16 (left) femurs with respect to four regions of interest (ROI). th.tb.: trabecular thickness (μm); BV/TV: trabecular bone volume (%); DA: degree of anisotropy; cv: coefficient of variation. ROI 1 samples the arcuate bundle; ROI 2 the medial end of the vertical bundle; ROI 3 the lateral end of the vertical bundle; ROI 4 the area included between the arcuate and the vertical bundles.

The four maps (Figure 1) reveal a highly comparable pattern of bone distribution between the right and the left femurs, the thickest values being located in both cases along the posterior, medial and lateral aspects of the proximal shaft, mainly along the *linea aspera* and the gluteal tuberosity. As shown by the virtually complete right specimen, the thinnest cortical bone is found towards the distal end of the diaphysis. In this case, the greatest cortical volume (CV) characterises the proximal portion of the shaft (79 % vs. 66 %), while of course the opposite is true for the medullary cavity (Table 2). Again, for the comparable variables, the degree of bilateral asymmetry is negligible.

Spy 9 (tibia)

The 3D cortical bone cartography of this left tibia is rendered in Figure 2. Here, the thickest bone is found along the anterior shaft
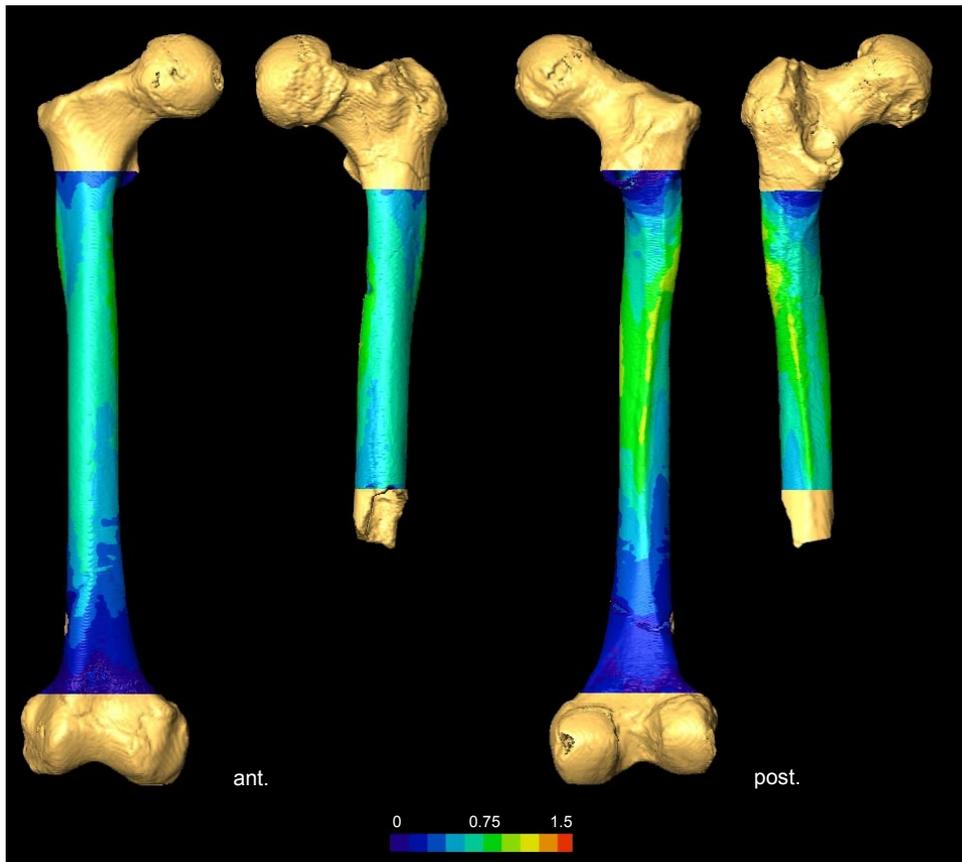

Figure 1. CT-based 3D mapping of the topographic distribution of the cortical bone thickness in the femurs Spy 8 (right, complete) and Spy 16 (left, proximal half) from the Spy II adult partial skeleton in anterior (left) and posterior (right) view. Images, not to scale, rendered by means of a 10-stepped chromatic scale.

	Spy 8 (r)	*Spy 16 (l)*	*Spy 9*
dCV (%)	24.31 (66.0)	-	16.50 (69.2)
dMV (%)	12.52 (34.0)	-	7.33 (30.8)
pCV (%)	27.39 (79.1)	27.66 (80.1)	16.68 (59.0)
pMV (%)	7.25 (20.9)	6.88 (19.9)	11.60 (41.0)

Table 2. Absolute (in cm³) and percent cortical (CV) and medullary (MV) volumes of the femurs Spy 8 (right) and Spy 16 (left), and the left tibia Spy 9 assessed for the distal portion (d) comprised between 35 % and 50 %, and for the proximal portion (p) between 50 % and 65 % of the relative estimated biomechanical length. r: right; l: left.

border, at mid-diaphysis, and postero-medially, along the soleal line. At least partially, the distribution map corresponds to the insertion areas of the muscles *tibialis anterior*, *soleus*, and *flexor digitorum longus*. As shown by the values in Table 2 (last column), a slight proportional increase in cortical volume (CV) can be observed towards the distal end (%pCV vs. %dCV).

Compared to the figures reported for the extant human tibia (Mazurier *et al.*, 2004, 2005; Mazurier, 2006), the articular plateau of this Neandertal specimen is proportionally and absolutely thick (Table 3) and thicker than La Ferrassie 2 (Mazurier & Macchiarelli, 2006). As

thick.	*MC*	*LC*
N	1873	2137
mean	2.69	2.26
s.d.	1.25	1.24
min.	0.24	0.15
max.	6.02	6.20

Table 3. Descriptive statistics of the cortico-trabecular complex (CCT) thickness variation (mm) of the Spy 9 tibial plateau measured on the medial (MC) and the lateral (LC) condyles.

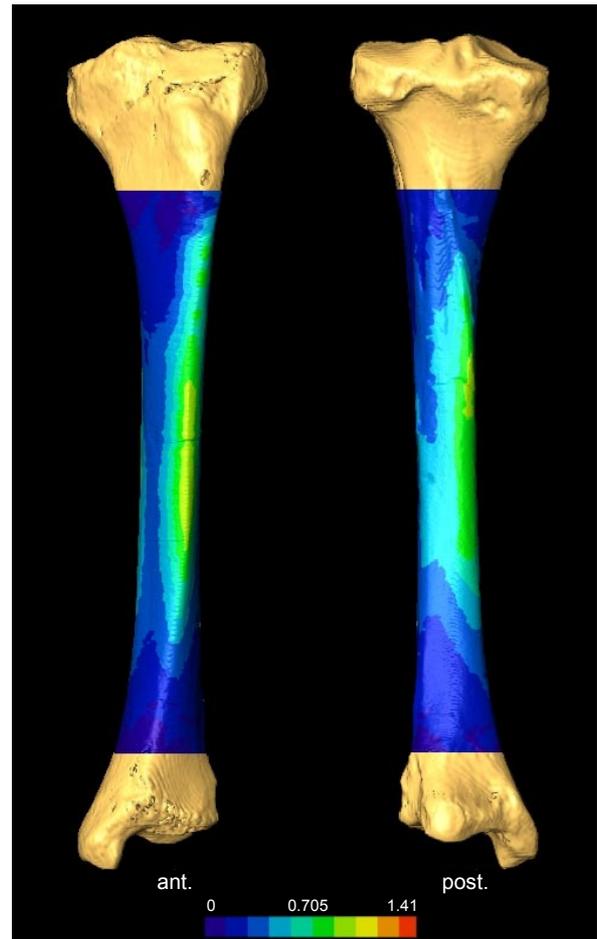

ant.   post.

0   0.705   1.41

Figure 2. CT-based 3D mapping of the topographic distribution of the cortical bone thickness in the left tibia Spy 9 from the Spy II adult partial skeleton in anterior (left) and posterior (right) view. Images, not to scale, rendered by means of a 10-stepped chromatic scale.

observed in modern human samples (Mazurier, 2006), Spy 9 medial condyle is, on average, thicker than the lateral one (2.7 vs. 2.3 mm), even if the absolute thickest value (6.2 mm) is found laterally.

The virtual rendering of the CTC topographic distribution of the young adult tibia from Spy II is shown in Figure 3. On the medial condyle, an antero-posteriorly extended reinforcement can be observed along the central and the antero-medial portions; on the lateral condyle, a strengthened CTC is set towards the posterior half, the thickest values being located towards the postero-medial portion.
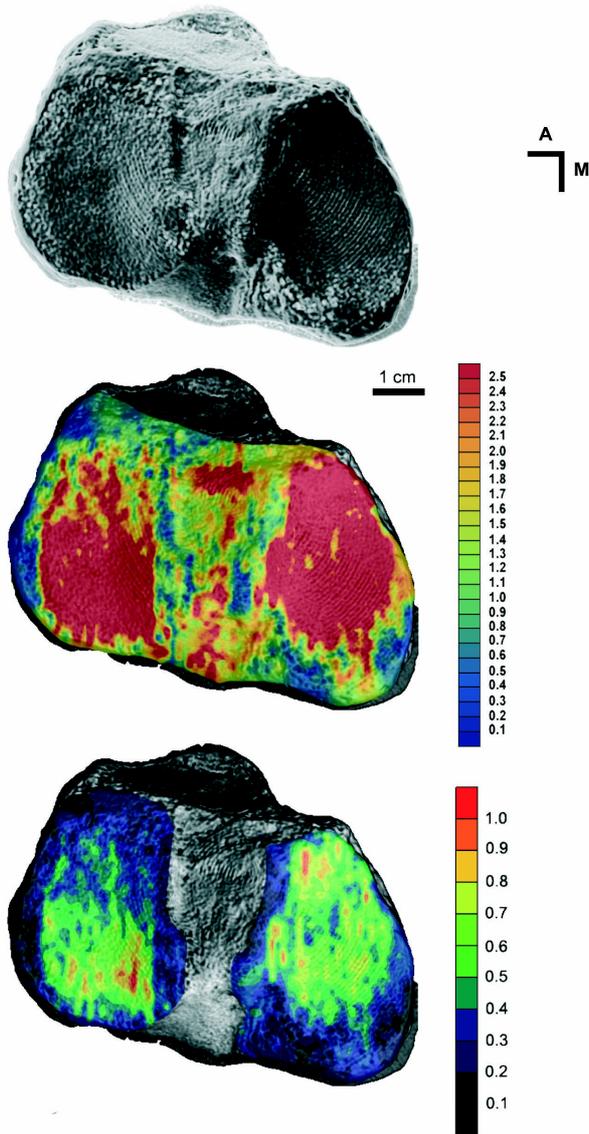
Figure 3. CT-based 3D reconstruction of the Spy 9 tibial plateau in superior view (top); map of the topographic distribution of the cortico-trabecular complex (CTC) thickness variation (scale in mm) (middle); distribution map of the coefficient of the mean maximal thickness (bottom). Maps rendered by means of a selected chromatic scale.

The variogram analysis of the two condylar components shows that both are spatially, locally and globally, very structured, characterised by strong heterogeneity and abrupt thickness variation, and similar intensity (Mazurier, 2006).

DISCUSSION AND CONCLUSIONS

As revealed by the noninvasive virtual analysis of their diaphyseal endostructural morphology, femoral cortical thickness distribution and bilateral asymmetry of bone volume, the latter being compatible with the reference Neandertal values provided by Trinkaus and co-workers (1994), confirm that Spy 8 and Spy 16 belong to the same individual, Spy II (Rougier *et al.*, 2004, this volume: chapter XIX). As regards to trabecular architecture, while relative bone density is not a reliable indicator when dealing with the fossil record (e.g. Macchiarelli *et al.*, 1999), the general textural arrangement of the cancellous network of the two proximal ends is compatible with this interpretation. Nonetheless, some differences in angular orientation and degree of anisotropy of the vertical bundle and site-specific strut thickness, apparently free from diagenetic changes, suggest a slightly unbalanced load distribution between the two sides, a pattern which deserves confirmation by additional higher-resolution 3D analyses.

Three-dimensional bone thickness topographic variation along the two femoral shafts points to a distinct medio-lateral reinforcement of the proximal half, a finding which supports previous observations on bending strength based on 2D cross-sectional geometry of the femoral shaft (Trinkaus & Ruff, 1989b). Bone distribution basically traces the topography of the muscles involved in the movements of rotation, extension, and adduction of the thigh, i.e., the *vastus intermedius*, on the anterior aspect of the femur, the *vastus lateralis* and *medialis*, the *adductor magnus* and *brevis*, and the short head of the *biceps femoris*, around the *linea aspera*, and, below the greater trochanter, the *gluteus maximus*, which relative development was originally described by Fraipont & Lohest (1886, 1887).

A comparable model of cortical bone distribution has been described for the femur of the Neandertal child from Roc de Marsal (Volpato *et al.*, 2007), whose age at death has been recently refined to the interval 2.5-3 years (Bayle *et al.*, 2009). In this immature individual, who already shows typically thickened bone and contracted medullary cavity (for the adult condition, see Ruff *et al.*, 1994), the femoral shaft is structurally reinforced compared to the average modern human condition, especially proximally. Similarly to the

6

adult Neandertal femora (Trinkaus & Ruff, 1989a, 1999a; Ruff *et al.*, 1993), the Roc de Marsal 1's endostructural morphology suggests proportionally greater medio-lateral bending strength near the midshaft (Volpato *et al.*, 2007). Nonetheless, relative to Roc de Marsal 1, bone volume distribution recorded for the young adult Spy II is more contrasted between the proximal and distal portions of the shaft, a pattern likely related to relative muscular development occurring later during growth.

Because of the current lack of similar 3D virtual reconstructions, no comparisons are possible with this respect between Spy 9 and an immature Neandertal tibia.

Compared to the values from the left tibial plateau of the adult La Ferrassie 2 skeleton (Mazurier, 2006; Mazurier & Macchiarelli, 2006; Mazurier *et al.*, 2006), the cortico-trabecular complex of Spy 9 is about 3 mm thicker, an evidence suggesting more strenuous levels of physical activity experienced by the latter, and/or individual- or, more likely, sexual-related variation.

As a whole, the results scattered from the 3D virtual modeling of the lower limb long bones (femurs and tibia) of the Spy II partial skeleton confirm the informative value of this kind of investigative approach, which is complementary to cross-sectional analyses (Trinkaus & Ruff, 1989b), in reconstructing loading histories from fossil specimens, including the assessment of habitual mechanical loads and patterns of physical activity.

ACKNOWLEDGEMENTS

BIBLIOGRAPHY

BAYLE P., BRAGA J., MAZURIER A. & MACCHIARELLI R., 2009. Dental developmental pattern of the Neanderthal child from Roc de Marsal: a high-resolution 3D analysis. *Journal of Human Evolution*, **56**: 66-75.

BEAUVAL C., MAUREILLE B., LACRAMPE-CUYAUBÈRE F., SERRE D., PERESSINOTTO D., BORDES J.-G., COCHARD D., COUCHOUD I., DUBRASQUET D., LAROULANDIE V., LENOBLE A., MALLYE J.-B., PASTY S., PRIMAULT J., ROHLAND N., PÄÄBO S. & TRINKAUS E., 2005. A late Neandertal femur from Les Rochers-de-Villeneuve, France. *Proceedings of the National Academy of Sciences USA*, **102**: 7085-7090.

CHURCHILL S. E., 1998. Cold adaptation, heterochrony, and Neandertals. *Evolutionary Anthropology*, **7**: 46-61.

CHURCHILL S. E. & SCHMITT D., 2002. Biomechanics in palaeoanthropology: engineering and experimental approaches to the study of behavioural evolution in the genus *Homo*. *In*: C. S. HARCOURT-SMITH & B. R. SHERWOOD (ed.), *New Perspectives in Primates Evolution and Behaviour*. Otley, Westbury Academic & Scientific Publishing: 71-102.

COWGILL L. W. & HAGER L. D., 2007. Variation in the development of postcranial robusticity: an example from Çatalhöyük, Turkey. *International Journal of Osteoarchaeology*, **17**: 235-252.

DALSTRA M. & HUISKES R., 1995. Load transfer across the pelvic bone. *Journal of Biomechanics*, **28**: 715-724.

DEAN C. & WOOD B., 2003. *A Digital Radiographic Atlas of Great Ape Skull and Dentition. Digital Archives of Human Paleobiology, 3*. Rome, Museo Nazionale "L. Pigorini" (CD-ROM, ISBN 88-87563-02-0).

FRAIPONT J. & LOHEST M., 1886. La race humaine de Néanderthal ou de Canstadt, en Belgique. Recherches ethnologiques sur des ossements humains, découverts dans des dépôts quaternaires d'une grotte à Spy et détermination de leur âge géologique. Note préliminaire. *Bulletin de l'Académie royale des Sciences de Belgique*, 3ème série, **XII**: 741-784.

FRAIPONT J. & LOHEST M., 1887. La race humaine de Néanderthal ou de Canstadt en Belgique. Recherches ethnologiques sur des ossements humains, découverts dans des dépôts quaternaires d'une grotte à Spy et détermination de leur âge géologique. *Archives de Biologie*, **7**/1886: 587-757.

GRINGARTEN E. & DEUTSCH C. V., 2001. Variogram interpretation and modeling. *Mathematical Geology*, **33**: 507-534.

GUMIAUX C., GAPAIS D. & BRUN J. P., 2003. Geostatistics applied to best-fit interpolation of orientation data. *Technophysics*, **376**: 241-259.

LOVEJOY C. O. & TRINKAUS E., 1980. Strength and robusticity of the Neandertal tibia. *American Journal of Physical Anthropology*, **53** (4): 465-470.

MACCHIARELLI R. & BONDIOLI L., 1994. Linear densitometry and digital image processing of proximal femur radiographs: implications for archaeological and forensic anthropology. *American Journal of Physical Anthropology*, **93** (1): 109-122.

MACCHIARELLI R., BONDIOLI L., GALICHON V. & TOBIAS P. V., 1999. Hip bone trabecular architecture shows uniquely distinctive locomotor behaviour in South African australopithecines. *Journal of Human Evolution*, **36**: 211-232.

MACCHIARELLI R., MAZURIER A. & VOLPATO V., 2007. L'apport des nouvelles technologies à l'étude des Néandertaliens. *In*: B. VANDERMEERSCH & B. MAUREILLE (ed.), *Les Néandertaliens. Biologie et Cultures*. Paris, Comité des Travaux Historiques et Scientifiques: 169-179.

MACCHIARELLI R., ROOK L. & BONDIOLI L., 2001. Comparative analysis of the iliac trabecular architecture in extant and fossil primates by means of digital image processing techniques: implications for the reconstruction of fossil locomotor behaviours. *In*: L. DE BONIS, G. D. KOUFOS & P. ANDREWS (ed.), *Hominoid Evolution and Climatic Change in Europe. Phylogeny of the Neogene Hominoid Primates of Eurasia*. Cambridge, Cambridge University Press: 60-101.

MARTINÓN-TORRES M., 2003. Quantifying trabecular orientation in the pelvic cancellous bone of modern humans, chimpanzees, and the Kebara 2 Neanderthal. *American Journal of Human Biology*, **15**: 647-661.

MAZURIER A., 2006. *Relations entre comportement locomoteur et variation cortico-trabéculaire du plateau tibial chez les primates: analyse quantitative non-invasive à haute résolution (SR-µCT) et applications au registre fossile*. Thèse de doctorat, Université de Poitiers: 388 p.

MAZURIER A., BONDIOLI L., BRAVIN A., NEMOZ C. & MACCHIARELLI R., 2004. L'empreinte du comportement locomoteur dans l'organisation structurale fine du plateau tibial. *Bulletins et Mémoires de la Société d'Anthropologie de Paris*, **16**: 235 (abstract).

MAZURIER A., BONDIOLI L., BRAVIN A., NEMOZ C. & MACCHIARELLI R., 2005. High-resolution (3D SR-µCT-based) structural analysis of the primate proximal tibia: evidence for locomotion-related topographic variation. *American Journal of Physical Anthropology*, suppl. **40**: 147 (abstract).

MAZURIER A. & MACCHIARELLI R., 2006. Spécificités endo-structurales du plateau tibial néandertalien. Analyse à haute-résolution du spécimen La Ferrassie 2. *Bulletins et Mémoires de la Société d'Anthropologie de Paris*, **18**: 233-234 (abstract).

MAZURIER A., NAKATSUKASA M., BONDIOLI L., ROOK L. & MACCHIARELLI R., 2007. Structural signature of bipedal training in the tibial plateau of a Japanese macaque. *American Journal of Physical Anthropology*, suppl. **43**: 167 (abstract).

MAZURIER A., VOLPATO V. & MACCHIARELLI R., 2006. Improved noninvasive microstructural analysis of fossil tissues by means of SR-microtomography. *Applied Physics A, Materials Science & Processing*, **83**: 229-233.

ODGAARD A., 1997. Three dimensional methods for quantification of cancellous bone architecture. *Bone*, **20**: 315-328.

ODGAARD A., KABEL J., VAN RIETBERGEN B., DALSTRA M. & HUISKES R., 1997. Fabric and elastic principal directions of cancellous bone are closely related. *Journal of Biomechanics*, **30**: 487-495.

PARFITT A. M., DREZNER M. K., GLORIEUX F. H., KANIS J. A., MALLUCHE H., MEUNIER P. J., OTT S. M. & RECKER R., 1987. Bone histomorphometry: standardization of nomenclature, symbols, and units. Report of the ASBMR histomorphometry nomenclature committee. *Journal of Bone and Mineral Research*, **2**: 595-609.

PEARSON O. M. & LIEBERMAN D. E., 2004. The aging of Wolff's "law": ontogeny and responses to mechanical loading in cortical bone. *Yearbook of Physical Anthropology*, **47**: 63-99.

ROUGIER H., CREVECOEUR I., FIERS E., HAUZEUR A., GERMONPRÉ M., MAUREILLE B. & SEMAL P., 2004. Collections de la Grotte de Spy: (re)découvertes et inventaire anthropologique. *Notae Praehistoricae*, **24**: 181-190.

RUFF C. B., 2002. Long bone articular and diaphyseal structure in old world monkeys and apes. I: locomotor effects. *American Journal of Physical Anthropology*, **119** (4): 305-342.

RUFF C. B., HOLT B. & TRINKAUS E., 2006. Who's afraid of the big bad Wolff? "Wolff's law" and bone functional adaptation. *American Journal of Physical Anthropology*, **129** (4): 484-498.

RUFF C. B., TRINKAUS E., WALKER A. & LARSEN C. S., 1993. Postcranial robusticity in *Homo*. I: temporal trends and mechanical interpretation. *American Journal of Physical Anthropology*, **91** (1): 21-53.

RUFF C. B., WALKER A. & TRINKAUS E., 1994. Postcranial robusticity in *Homo*. III: Ontogeny. *American Journal of Physical Anthropology*, **93** (1): 35-54.

RUIMERMAN R., HILBERS P., VAN RIETBERGEN B. & HUISKES R., 2005. A theoretical framework for strain-related trabecular bone maintenance and adaptation. *Journal of Biomechanics*, **38**: 931-941.

SEMAL P., TOUSSAINT M., MAUREILLE B., ROUGIER H., CREVECOEUR I., BALZEAU A., BOUCHNEB L., LOURYAN S., DE CLERCK N. & RAUSIN L., 2005. Numérisation des restes humains néandertaliens belges. Préservation patrimoniale et exploitation scientifique. *Notae Praehistoricae*, **25**: 25-38.

SLÁDEK V., BERNER M. & SAILER R., 2006. Mobility in Central European late Eneolitic and early Bronze Age: femoral cross-sectional geometry. *American Journal of Physical Anthropology*, **130** (3): 320-332.

SPARACELLO V. & MARCHI D., 2008. Mobility and subsistence economy: a diachronic comparison between two groups settled in the same geographical area (Liguria, Italy). *American Journal of Physical Anthropology*, **136** (4): 485-495.

SPOOR C. F., ZONNEVELD F. & MACHO G., 1993. Linear Measurements of cortical bone and dental enamel by computed tomography: applications and problems. *American Journal of Physical Anthropology*, **91** (4): 469-484.

STOCK J. T., 2006. Hunter-gatherer postcranial robusticity relative to patterns of mobility, climatic adaptation, and selection for tissue economy. *American Journal of Physical Anthropology*, **131** (2): 194-204.

STOCK J. & PFEIFFER S., 2001. Linking structural variability in long bone diaphyses to habitual behaviors: foragers from the Southern African Later Stone Age and the Andaman Islands. *American Journal of Physical Anthropology*, **115** (3): 337-348.

STOCK J. T. & PFEIFFER S. K., 2004. Long bone robusticity and subsistence behavior among later Stone Age foragers of the forest and fynbos biomes of South Africa. *Journal of Archaeological Science*, **31**: 999-1013.

TRINKAUS E., CHURCHILL S. E. & RUFF C. B., 1994. Postcranial robusticity in *Homo*. II: humeral bilateral asymmetry and bone plasticity. *American Journal of Physical Anthropology*, **93** (1): 1-34.

TRINKAUS E., CHURCHILL S. E. & RUFF C. B., 1999. Long bone shaft robusticity and body proportions of the Saint-Césaire 1 Châtelperronian Neanderthal. *Journal of Archaeological Science*, **26**: 753-773.

TRINKAUS E. & RUFF C. B., 1989a. Cross-sectional geometry of Neandertal femoral and tibial diaphyses: implications for locomotion. *American Journal of Physical Anthropology*, **78**: 315-316 (abstract).

TRINKAUS E. & RUFF C. B., 1989b. Diaphyseal cross-sectional morphology and biomechanics of the Fond-de-Forêt 1 femur and the Spy 2 femur and tibia. *Anthropologie et Préhistoire*, **100**: 33-42.

TRINKAUS E. & RUFF C. B., 1999a. Diaphyseal cross-sectional geometry of Near Eastern Middle Palaeolithic humans: the femur. *Journal of Archaeological Science*, **26**: 409-424.

TRINKAUS E. & RUFF C. B., 1999b. Diaphyseal cross-sectional geometry of Near Eastern Middle Paleolithic humans: the tibia. *Journal of Archaeological Science*, **26**: 1289-1300.

TRINKAUS E., RUFF C. B. & CHURCHILL S. E., 1998. Locomotion and body proportions of the Saint-Césaire 1 Châtelperronian Neandertal. *Proceedings of the National Academy of Sciences USA*, **95**: 5836-5840.

VOLPATO V., 2007. *Morphogenèse des propriétés texturales du tissu osseux et environnement biomécanique. Caractérisation non invasive du réseau trabéculaire et de l'os cortical du squelette appendiculaire de mammifères actuels et fossiles, hominidés inclus*. Thèse de doctorat, Université de Poitiers: 339 p.

VOLPATO V., 2008. Morphogenèse de l'endostructure osseuse de l'ilion humain (*Engl. version*: Bone endostructure morphogenesis of the human ilium). *Comptes Rendus Palevol*, **7**: 463-471.

VOLPATO V., COUTURE C., MACCHIARELLI R. & VANDERMEERSCH B., 2011. Endostructural characterisation of the Regourdou 1 Neanderthal proximal arm: bilateral asymmetry and handedness. *In*: S. CONDEMI & G.-C. WENIGER (ed.), *Continuity and discontinuity in the peopling of Europe. One hundred fifty years of Neanderthal study*. Dordrecht, Springer: 175-178.

VOLPATO V., RUFF C., MACCHIARELLI R. & COWGILL L., 2007. Cross-sectional geometry of the Roc de Marsal juvenile Neandertal femur, determined using high-resolution microtomography. *American Journal of Physical Anthropology*, suppl. **43**: 240 (abstract).

VOLPATO V., VIOLA T. B., NAKATSUKASA M., BONDIOLI L. & MACCHIARELLI R., 2008. Textural characteristics of the iliac-femoral trabecular pattern in a bipedally-trained Japanese macaque. *Primates*, **49**: 16-25.

WEAVER T. D., 2003. The shape of the Neandertal femur is primarily the consequence of a hyperpolar body form. *Proceedings of the National Academy of Sciences USA*, **100**: 6926-6929.

ZOLLIKOFER C. P. E. & PONCE DE LEÓN M. S., 2001. Computer-assisted morphometry of hominoid fossils: the role of morphometric maps. *In*: L. DE BONIS, G. D. KOUFOS & P. ANDREWS (ed.), *Hominoid Evolution and Climatic Change in Europe. Vol. 2. Phylogeny of the Neogene Hominoid Primates of Eurasia*. Cambridge, Cambridge University Press: 50-59.

AUTHORS AFFILIATION

Virginie VOLPATO
Senckenberg Forschungsinstitut
und Naturmuseum
Senckenberganlage 25
60325 Frankfurt am Main
Germany
vvolpato@senckenberg.de

Arnaud MAZURIER
Société Études Recherches Matériaux (E.R.M.)
CRI Biopole
86000 Poitiers
France
arnaud.mazurier@erm-poitiers.fr

Laurent PUYMERAIL
Roberto MACCHIARELLI
UMR 7194
Département de Préhistoire
du Muséum national d'Histoire naturelle
43, rue Buffon
75005 Paris
France
laurent.puymerail@mnhn.fr
roberto.macchiarelli@mnhn.fr

Roberto MACCHIARELLI
Département Géosciences
Université de Poitiers
rue A. Turpain, bât. B8
86022 Poitiers
France
roberto.macchiarelli@univ-poitiers.fr